CHARACTERIZATION OF THE ELASTO-KINEMATIC BEHAVIOR OF GENERALIZED CROSS-SPRING BEARINGS

Gonçalves Junior, L.A.;Bitencourt, A.C.P**;Theska, R.***;Lepikson,H.A.*****

Centro Integrado de Manufatura e Tecnologia da Bahia
*Area of Industrial Product Development, E-mail: luis.antonio@fieb.org.br
****Institute SENAI of Innovation in Automation
**Instituto Federal da Bahia, Department of Mechanical Engineering
***Technische Universität Ilmenau, Institute of Design and Precision Engineering

ABSTRACT

Cross-spring bearings are widely used in precision engineering applications due to the high repeatability of motion and systematic characteristic of the main errors. Thus, this work is focused in the characterization of the elasto-kinematic behavior of such bearings. Firstly, an analytical approached is proposed to model load-rotation relationship of cross-spring bearings. Then, a numeric-iterative technique is used to obtain the solution of the resulting nonlinear system of equations. The obtained results are used to determine the major systematic error of the bearing; the rotary axis deviation. Furthermore, they are also applied to perform the geometric optimization, stress analyzes and to investigate the stiffness characteristics in order to provide useful insights to help in design stage of such a bearing. Finally, the results provided by the mathematic model are verified by finite element analyzes (FEA).

Index Terms **–** Cross-spring Bearing, Complaint Mechanism, Finite Element Analyzes, Precision Engineering

1. INTRODUCTION

Generalized cross-spring bearings are constructive elements composed of two in-angle leaves crossing at an arbitrary point of their length, see Figure 1. They provide relative rotation between two adjacent rigid members, through bending. Due to their advantages over the conventional bearings, such as substantially diminished friction (just internal bonding forces), no backlash, absence of stick slip (infinitesimal resolution), high repeatability, ease assembly and maintenance-free [1]–[9] cross-spring bearings are widely used in several applications of precision engineering field, positioning and manipulation systems, in metrology (balances, dynamometers, seismometers and pressure transducers), optical instrumentation and gyroscopes [4], [7]–[9].

On the other hand, the strongly limited range of motion of such a bearing rises as the main drawback of its use. Furthermore, they do not provide a pure rotation around a fixed rotary axis because of its complex elastic-kinematic behavior [1]–[4], [8]–[11].

When cross spring bearings are required to high precision applications, its elasto-kinematic behavior has to be known in order to compensate systematic errors. Moreover, a detailed knowledge of the cross-spring bearings overall behavior may allow a design optimization suitable to each applications.

Many different approaches of modeling the elasto-kinematic behavior of cross-spring bearings can be found. Most of them are restricted to symmetric cross-spring; others are not

suitable to help in the prediction of systematic errors. They apply different approaches such as: kinematic mechanism [10], pseudo-rigid-body [4], [6], elliptical integral to solve the exact Euler-Bernoulli elastic equation [11], among others. Only a few of the existent approaches fulfill at the same time the requirements of providing a parametric optimization to help the design of the bearing and to predict systematics behavior to support further compensations [3], [5].

In the present work is presented an intermediary solution between the analytical approach restricted to symmetric cross-spring bearings proposed by [8] and the generalized parametric approach provided by [3], which makes use of series approximations presented by [12]. Thus, this paper focuses firstly on the development of a mathematical model to characterize the elasto-kinematic behavior of generalized cross-spring bearings submitted to a coplanar general condition of loads (bending moment, vertical and horizontal loads). Then, the parameters resulted from this model are applied to predict the deviation of its rotary axis and to evaluate the influence of its geometric parameters over this parasite motion, aiming the bearings geometric optimization through the minimization of this deviation. Furthermore, this model is used to analyze the influence of these geometric parameters and the external vertical and horizontal loads over the rotational stiffness and stress characteristics of such a bearing, with the purpose of predicting its motion capability. Finally the results provided by the proposed mathematic model are verified by finite element analysis (FEA).

2. DEVELOPED MATHEMATIC MODEL

First of all, to model the elasto-kinematic characteristics of a generalized cross-spring bearing it is necessary to define its geometric parameters and the shape parameters of its leaves, see Figure 1 (a) and (b) respectively.

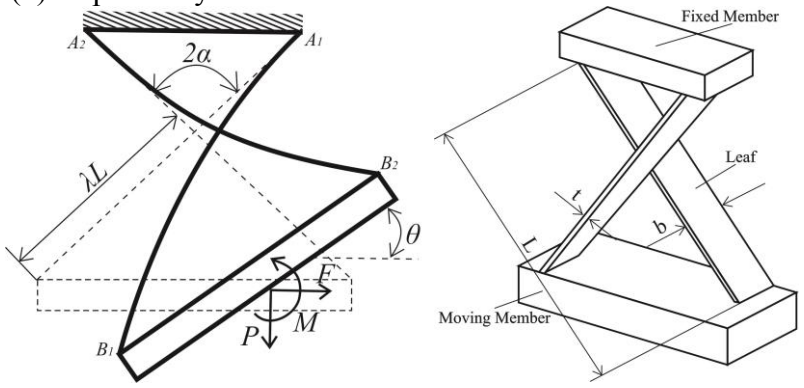

***Figure 1**: Generalized cross spring bearing - (a) geometric parameters, (b) shape parameters*

The shape parameters are defined as: *L*,*b*,*t,* length, width and thickness respectively.

On the other hand, the geometric parameters are: λ defined in the range of [0,1] determines the intersection point of the leaves in the initial state and α defined in the range of [0,π/2] determines the semi-angle between the leaves.

For the sake of mathematical convenience the following non-dimensional parameters are introduced.

$$m_i = \frac{M_i L}{EI_z},\ f_i = \frac{F_i L^2}{EI_z},\ p_i = \frac{P_i L^2}{EI_{zi}},\ \delta y_i = \frac{\Delta y_i}{L},\ \delta x_i = \frac{\Delta x_i}{L},\ y_i = \frac{Y_i}{L},\ x_i = \frac{X_i}{L},\ 1 = \frac{L}{L},$$

$$dx = \left(\frac{DX}{L}\right),\ dy = \left(\frac{DY}{L}\right),\ d = \left(\frac{D}{L}\right),\ k = \frac{KL}{EI_z},\ y_s = \left(\frac{2Y_s}{t}\right),\ s = 12\left(\frac{L}{t}\right)^2$$

Where E is the Young's modulus and I_{zi} the moment of inertia relative to OZ_i axis.

In the following the lower case letter will be used to denote non-dimensional quantities, while the upper case letter to express dimensional parameters. The subscript *i* will be used to describe the two leaves and quantities related to them.

2.1 Load-rotational relationship of generalized cross-spring bearings

When the moving member undergoes a coplanar general condition of load *M*, *F* and *P* – bending moment, horizontal and vertical loads respectively – it suffers a rotation θ relative to the fixed member. In response to this movement the leaves react to the applied external loads and deflect from ΔX_i and ΔY_i so that the equilibrium condition is reestablished. Thus, from the rigid body diagram showed in Figure 2 the in plane equilibrium equations of the moving member can be written in global coordinate system as follow:

$$\overset{+}{\rightarrow}\sum f_x = 0 \therefore f = (p_2 - p_1)\sin(\alpha) + (f_1 + f_2)\cos(\alpha) \tag{1}$$

$$+\downarrow \sum p_y = 0 \therefore p = (p_1 + p_2)\cos(\alpha) + (f_1 - f_2)\sin(\alpha) \tag{2}$$

$$\begin{aligned} +\circlearrowleft \sum m_z = 0 \therefore m = m_1 + m_2 + \left[(p_1 - p_2)\cos(\alpha) + (f_1 + f_2)\sin(\alpha)\right]\lambda 1 \sin(\alpha)\cos(\theta) \\ -\left[(p_1 + p_2)\sin(\alpha) - (f_1 - f_2)\cos(\alpha)\right]\lambda 1 \sin(\alpha)\sin(\theta) \end{aligned} \tag{3}$$

Furthermore, from assumption that the distance between the two moving ends of the leaves is constant regardless the bearing deflection (fixed and moving members are rigid) comes up the geometric compatibility equations in *X* and *Y* direction respectively, expressed as follow:

$$(\delta y_1 - \delta y_2)\cos(\alpha) + (\delta x_1 + \delta x_2)\sin(\alpha) = 2\lambda 1 \sin(\alpha)(1 - \cos(\theta)) \tag{4}$$

$$(\delta y_1 + \delta y_2)\sin(\alpha) - (\delta x_1 - \delta x_2)\cos(\alpha) = 2\lambda 1 \sin(\alpha)\sin(\theta) \tag{5}$$

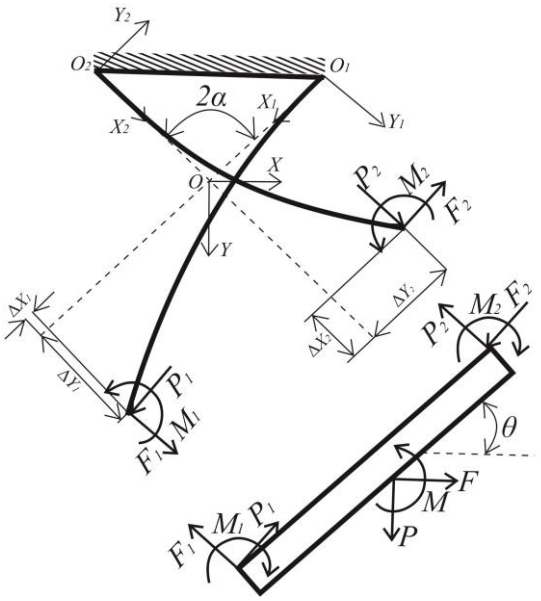

***Figure 2**: Load-displacement relationship of a generalized cross spring bearing*

Eqs. 1-5 are described into 11 unknown variables which define the elasto-kinematic behavior of the bearing: θ, f_1, f_2, p_1, p_2, m_1, m_2, δy_1, δy_2, δx_1 e δx_2.

Nevertheless, to determine these unknown variables a system of 11 equations is needed. Thus, the remaining six equations are obtained from the Euler-Bernoulli differential equation, which define the load-displacement relationship of the leaf, see Figure 3.

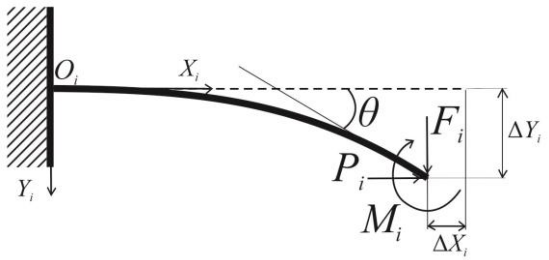

***Figure 3**: Load-displacement relationship of the leaf*

$$EI\frac{d^2Y_i\left(X_i\right)/dX_i^{\,2}}{\left[1+\left(dY_i\left(X_i\right)/dX_i\right)^2\right]^{3/2}}=-P_i\left(\Delta Y_i-Y_i\left(X_i\right)\right)+F_i\left(L-X_i\right)+M_i,\ \ i=1,2 \tag{6}$$

Solutions of Eq. 6 can be obtained in terms of elliptical integrals [11]. However, this principle of solution leads to a lengthy iterative procedure with high computational cost. Thus, to small deflection angles Eq. 6 can be linearized by neglecting the high order terms, resulting in:

$$EI\frac{d^2}{dX_i^{\,2}}Y_i\left(X_i\right)=-P_i\left(\Delta Y_i-Y_i\left(X_i\right)\right)+F_i\left(L-X_i\right)+M_i,\ \ i=1,2 \tag{7}$$

Finally, using the non-dimensional relationship previously presented Eq. 7 can be written in the dimensionless form, as follows:

$$\frac{d^2}{dx_i^{\,2}}y_i\left(x_i\right)=-p_i\left(\delta y_i-y_i\left(x_i\right)\right)+f_i\left(1-x_i\right)+m_i,\ \ i=1,2 \tag{8}$$

To solve Eq. 8 the following boundary conditions can be used:

$$y_i(0)=0,\ \ y_i'(0)=0,\ \ i=1,2$$

Thus, integrating Eq.8 twice and imposing the appropriated boundary conditions, the expressions for the transverse displacement and the slope angle along the leaves can be obtained. Therefore, through some mathematical manipulations the solutions can expressed in terms of hyperbolic functions as follows [9], [12]:

$$\begin{aligned}y_i(x_i)=f_i&\left[\frac{\cosh\left(\sqrt{p_i}x_i\right)}{p_i}-\frac{\sinh\left(\sqrt{p_i}x_i\right)}{p_i^{(3/2)}}+\frac{x_i}{p_i}-\frac{1}{p_i}\right]+m_i\left[\frac{\cosh\left(\sqrt{p_i}x_i\right)}{p_i}-\frac{1}{p_i}\right]\\&+\delta y_i\left[1-\cosh\left(\sqrt{p_i}x_i\right)\right],\ \ i=1,2\end{aligned} \tag{9}$$

$$y_i'(x_i) = f_i\left[\frac{\sinh\left(\sqrt{p_i}x_i\right)}{\sqrt{p_i}} - \frac{\cosh\left(\sqrt{p_i}x_i\right)}{p_i} + \frac{1}{p_i}\right] + \frac{m_i \sinh(\sqrt{p_i}x_i)}{\sqrt{p_i}} - \delta y_i \sqrt{p_i}\sinh\left(\sqrt{p_i}x_i\right),\ i=1,2 \tag{10}$$

Finally, the displacement δy_i and the rotational angle θ at the end of the leaves can be obtained by making x_i=1:

$$\delta y_i = f_i\left[\frac{\sqrt{p_i} - \tanh\left(\sqrt{p_i}\right)}{p_i^{(3/2)}}\right] + m_i\left[\frac{\cosh\left(\sqrt{p_i}\right)-1}{p_i\cosh\left(\sqrt{p_i}\right)}\right],\ i=1,2 \tag{11}$$

$$\theta \approx f_i\left[\frac{\cosh\left(\sqrt{p_i}\right)-1}{p_i\cosh\left(\sqrt{p_i}\right)}\right] + \frac{m_i\tanh\left(\sqrt{p_i}\right)}{\sqrt{p_i}},\ i=1,2 \tag{12}$$

From the six equations which describes the load-displacement relationship of the leaves the last two are related to the variation δx_i of their length along the OX_i axis. The δx_i displacement can be divided into two components: the first, known as kinematic component, is given by the constraint condition of constant arc length of the leaves: the second, known as elastic component, results from the purely elastic leaves stretching, due to the action of the normal loads p_i.

The kinematic component can be written through the integration of the leaves infinitesimal arc element, as follows:

$$\delta x_{ki} = \int_0^1 \left\{1 - \sqrt{1+\left[y'_i(x_i)\right]^2}\right\} dx_i \ \therefore\ \delta x_{ki} \approx -\frac{1}{2}\int_0^1 \left[y'_i(x_i)\right]^2 dx_i,\ i=1,2 \tag{13}$$

Thus, substituting Eq. 10 into Eq. 13 and performing the integration the kinematic component of δx_i can be obtained.

On the other hand, the elastic component may be obtained through the expression for the elastic stretching of an axially loaded member, as follows:

$$\delta x_{ei} = \frac{\Delta x_{ei}}{L}\ \therefore\ \delta x_{ei} = \frac{P_i}{EA_s}\ \therefore \delta x_{ei} = \frac{p_i}{s},\ i=1,2 \tag{14}$$

Where A_s is the leaves cross section area and s the non-dimensional parameter defined at the beginning of this section.

Finally, the expression for the δx_i variation is given by:

$$\delta x_i \approx -(\delta x_{ei} + \delta x_{ki}),\ i=1,2 \tag{15}$$

Producing:

$$\delta x_i \approx -\frac{p_i}{s} + f_i^2\left[\frac{10\sqrt{p_i}\cosh\left(\sqrt{p_i}\right)+2\sqrt{p_i}\cosh\left(3\sqrt{p_i}\right)-3\sinh\left(\sqrt{p_i}\right)-3\sinh\left(3\sqrt{p_i}\right)}{4p_i^{(5/2)}\cosh\left(3\sqrt{p_i}\right)+12p_i^{(5/2)}\cosh\left(\sqrt{p_i}\right)}\right] + f_i m_i\left[\frac{3\cosh\left(\sqrt{p_i}\right)-2\cosh\left(2\sqrt{p_i}\right)+\cosh\left(3\sqrt{p_i}\right)-\sqrt{p_i}\sinh\left(2\sqrt{p_i}\right)-2}{p_i^{\,2}\cosh\left(3\sqrt{p_i}\right)+3p_i^{\,2}\cosh\left(\sqrt{p_i}\right)}\right] + m_i^{\,2}\left[\frac{\sinh\left(\sqrt{p_i}\right)+\sinh\left(3\sqrt{p_i}\right)-4\sqrt{p_i}\cosh\left(\sqrt{p_i}\right)}{4p_i^{(3/2)}\cosh\left(3\sqrt{p_i}\right)+12p_i^{(3/2)}\cosh\left(\sqrt{p_i}\right)}\right],\ i=1,2 \quad (16)$$

The non-linear system formed by Eqs. 1-5, 12-13 and 16 can be solved using the Levenberg-Marquardt Algorithm, which proved to be efficient in solving medium-size non-linear problems even when the iterative procedure begins far from the final solution [9], [13]. To solve iteratively a system of equations an initial solution is needed. In this case, it was used the approximated solutions provided by [5] for the unknown variables θ, f_1, f_2, p_1, p_2, m_1, m_2, δy_1, δy_2 and those presented by [12] for the variables δx_1 and δx_2.

2.2 Rotary axis deviation

As aforementioned, the cross-spring bearing nonlinear behavior yields a deviation of its rotary axis. Figure 4 shows that this parasite motion can be characterized by the intersection of the straight lines tangent to the end of leaves. Therefore, knowing the position of points B_1 and B_2 as well as the leaves slope on these points (the same as the moving member angle θ) it is possible to define the equations of these straight lines.

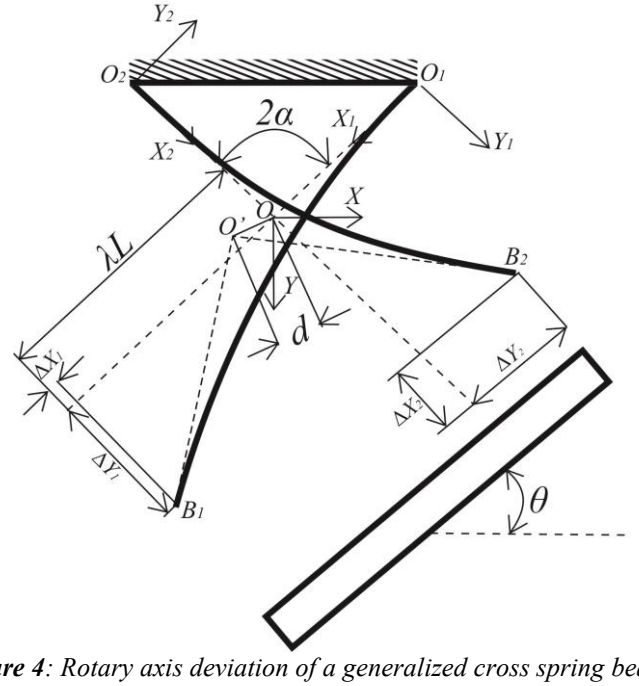

***Figure 4**: Rotary axis deviation of a generalized cross spring bearing*

Thus, the straight-line equations on the local coordinate system OXY_i, $i=1,2$ can be written as follows:

$$y_i - \delta y_i = \tan(\theta)(x_i - \delta x_i),\ i = 1,2 \tag{17}$$

The intersection point between the two straight lines can be determined by solving the linear system formed by their equations, which must be written at the same coordinate system. For the sake of mathematical convenience this system, called here as global coordinate system, is chosen as shown in Figure 4. The straight lines can be rewritten in global coordinate system by performing a rotation and subsequently a translatory transformation of coordinate systems, expressed as follows.

$$\begin{bmatrix} x_i \\ y_i \end{bmatrix} = \begin{bmatrix} -\sin(\alpha) & \cos(\alpha) \\ \cos(\alpha) & \sin(\alpha) \end{bmatrix} \begin{bmatrix} x_i' \\ y_i' \end{bmatrix},\ i = 1,2 \tag{18}$$

$$\begin{bmatrix} x_i' \\ y_i' \end{bmatrix} = \begin{bmatrix} x - 1(1-\lambda)\sin(\alpha) \\ y + 1(1-\lambda)\cos(\alpha) \end{bmatrix},\ i = 1,2 \tag{19}$$

Where x_i' and y_i' define a generic coordinate written in the intermediary coordinate system OXY'_i.

Then, substituting Eqs.18-19 into the Eq. 17 the expression of the straight lines can be expressed in global coordinate system OXY as:

$$x\left[\cos(\alpha) + \sin(\alpha)\tan(\theta)\right] + y\left[\sin(\alpha) - \cos(\alpha)\tan(\theta)\right] = \delta y_1 - \tan(\theta)(\lambda 1 + \delta x_1) \tag{20}$$

$$x\left[\cos(\alpha) - \sin(\alpha)\tan(\theta)\right] - y\left[\sin(\alpha) + \cos(\alpha)\tan(\theta)\right] = \delta y_2 - \tan(\theta)(\lambda 1 + \delta x_2) \tag{21}$$

Finally the normalized rotary axis deviation can be determined by:

$$d = \sqrt{x_p^{\,2} + y_p^{\,2}} \tag{22}$$

Where the point (x_p, y_p) is the solution of the system stated by Eqs. 20-21.

3. RESULTS AND DISCUSSION

3.1 Rotary axis deviation

The results obtained by the proposed model for the normalized axis deviation of a symmetric bearing loaded by pure moment (λ=0.5) were compared to those accepted as the most accurate solution provided by [11]. First of all, it is possible to see a good agreement between them, especially in small rotational angles of the moving member, see Figure 5. It is also noteworthy the progressively increase of the relative deviation between the results, which can be explained by adoption of the approximation taken in the expression for the leaf curvature, Eq. 6. In case, it was reached a maximum deviation less than 7.1%, which occurred when θ and α were 30º and 45º, respectively.

Further analyzes of the rotary axis deviation, including the cases in which the bearing is asymmetric and also loaded by external vertical force, are provided in the next section

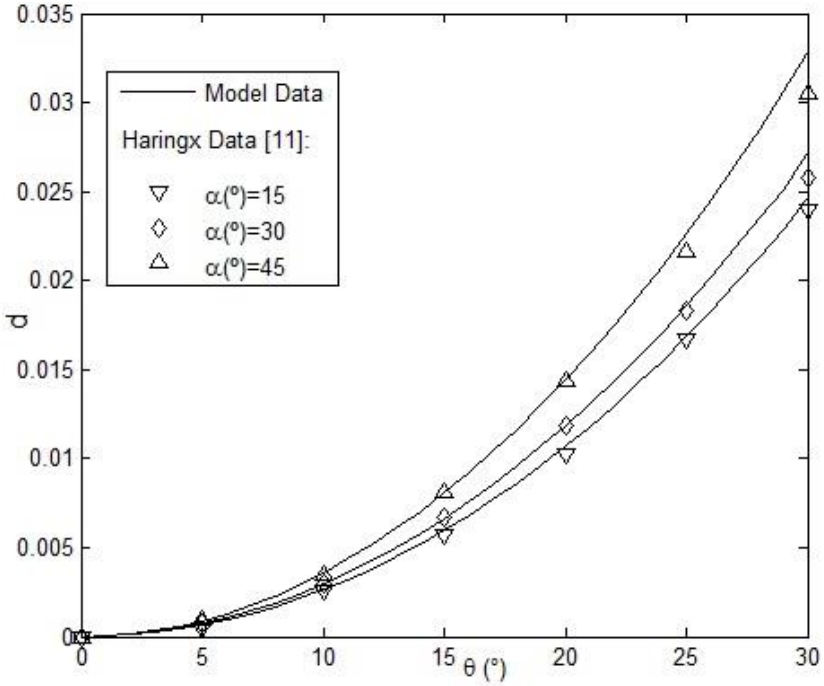

Figure 5*: Normalized axis deviation of a symmetric cross-spring bearing under a pure moment condition of load*

3.2 Geometrical optimization

Solutions of the nonlinear system formed by Eqs. 1-5, 11-12, and 16 allow the evaluation of the geometric parameters influence over the rotary axis deviation provided by Eq. 22.

Figure 6 shows the influence of parameter λ on this parasite motion when the bearing undergoes an angle of 15º produced by pure bending moment. In this case, it is possible to see that the axis deviation is strongly influenced by parameter λ. Furthermore, it is worth to note that when λ is 0.5 the axis deviation reaches its maximum. On the other hand, when λ is 12.77% or 87.81% this parasite motion is substantially minimized. Hongzhe and Shusheng achieved a similar result (λ = 12.7322% or 87.2678%) on their work [3].

Investigation of Figures 6 (a) also shows a tendency from curves profile when the geometric parameter α is varied, so that the minimum values of the axis deviation remains occurring when λ is 12.77% or 87.81%. Thus, for the sake of design optimization it is important an evaluation of α parameter influence on these two points.

Then, when λ is 12.77% the minimum axis deviation is provided by α nearly to 70º while this value is about 37.5º when λ is 87.81%, see Figures 6 (b) and (c) respectively. However, it is important to note in these curves that for small angles of rotation (up to 5º) the axis deviation is poorly influenced by the geometric parameter α.

The previous analyze regards to a pure moment state of load. However, it is not the load condition of most practical applications of cross-spring bearings.

The behavior of the geometric parameters is influenced by the action of the vertical load. Figure 7 (a) shows that when p is negative (compressive load) the values of λ which yields a minimum axis deviation displace in the direction of the symmetric bearing (λ=0.5), whereas when p is positive (tensile load) these values move in direction of the triangular geometries (λ=0 and 1).

Thus, it is not possible to establish an optimized geometric configuration in applications in which the bearing works in a condition of variable vertical load. On these cases, a reasonable geometric configuration can be determined performing the average of the λ values provided by the maximum and minimum vertical p, since the interval of p does not be great enough to produce a large discrepancy between the extreme λ values.

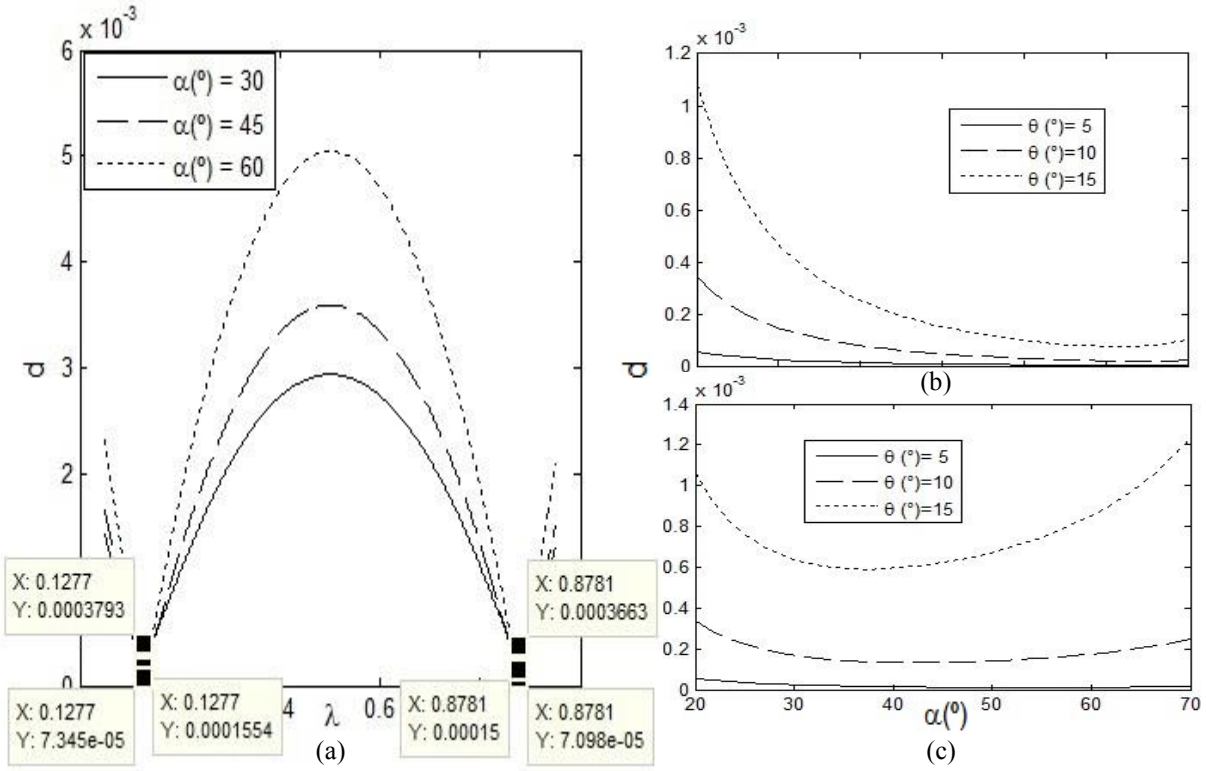

Figure 6*: Influence of the geometric parameters λ and α on the normalized rotary axis deviation when the bearing undergoes a pure moment of condition of load - (a) d against λ for α=30°,45° and 60°, (b) d against α for θ=5°,10° and 15° when λ=0.1277, (c) d against α for θ=5°,10° and 15° when λ=0.8781*

Thus, an example is given, tanking the values in vicinity of λ equal to 0.1277 and the range of vertical load p equal to [-0.6023, 1.205] (purposely asymmetrically chosen), see Figures 7. In this case, a reasonable value of λ for p varying in the interval can be obtained as follow:

$$\lambda_{med} = \frac{0.0914 + 0.1433}{2} \;\therefore\; \lambda_{med} \approx 0{,}1174 \tag{23}$$

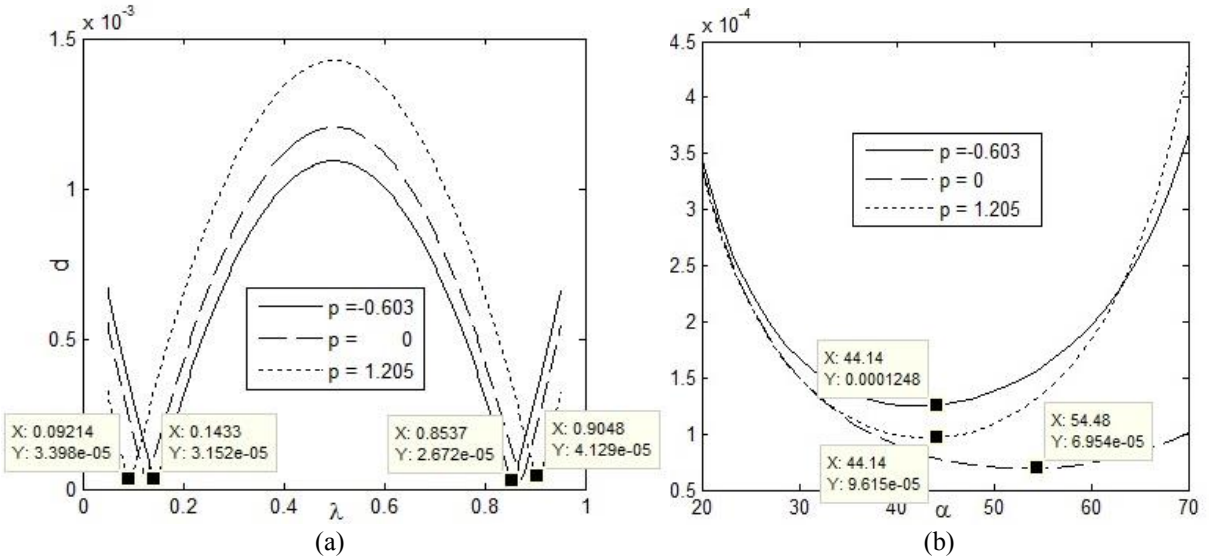

Figure 7*: Influence of the geometric parameters λ and α on the normalized rotary axis deviation when the bearing is submitted to the action of the vertical load p - (a) d against λ for p=-0.603, 0 and 1.205, (b) d against α for p=-0.603, 0 and 1.205 when λ=0.1174*

Analogously to the case in which the bearing undergoes a pure moment condition of load, when the vertical load is applied the geometric parameter α presents less influence on the axis deviation than λ. Therefore, a reasonable value for α in this situation can be obtained by using λ=0.1174 as calculated before.

Figure 7 (b) shows for the condition of vertical load defined in the example that for cases in which the p load is of compression or tension the minimum axis deviation is produced by α nearly to 44 º. On the other hand, in absence of p this value is about 55º. However, it is noteworthy that in this case the axis deviation is poorly influenced by values of α within the range of [40º,70º]. Thus, for convenience of symmetry it is reasonable to adopt a value of 45º to α in this situation.

3.3 Stiffness characteristics

As presented in the previous section for the geometric optimization, an analysis of the bearing rotational stiffness can be also performed from the solutions of the nonlinear system formed by Eqs.1-5, 11-12, and 16.

The bearing rotational stiffness can be readily defined as the ratio between the external moment applied to the bearing moving member and its rotational angle.

$$K = \frac{M}{\theta} \tag{24}$$

Figure 8 shows that the rotational stiffness is minimum (greatest compliance) when the bearing is symmetric (λ=0.5) and maximum when it assumes a triangular geometric configuration (λ = 0 or 1). Furthermore, it is possible to see that α has a negligible influence on the rotational stiffness when the bearing is loaded with pure bending moment.

On the other hand, evaluation of Figure 9 (a) shows that the rotational stiffness is less influenced by the variation of the vertical load p for bearings with $\lambda \in [0,0.5]$ than their symmetrical correspondents (e.g. λ=0.1277 and 0.8781). Furthermore, Figure 9 (b) shows, as expected, a less influence of α parameter on the stiffness when p is varied.

Rotational stiffness is also influenced by horizontal load applied to the bearing moving member. Figure 10 shows that for the symmetric bearing the stiffness is progressively reduced when horizontal load is increased [7]. This conclusion can be, without loss of generality, extended to any bearing geometric configuration. Then, the application of such load should be avoided for most practical application, considering that its effect leads to the decrease of the bearing stability, resulting, in extremes cases, in negative stiffness, which represents physically the geometric instability of the bearing. Besides that, the practical effects of rotational motion provided by the horizontal load can be replaced by a moment of proportional magnitude.

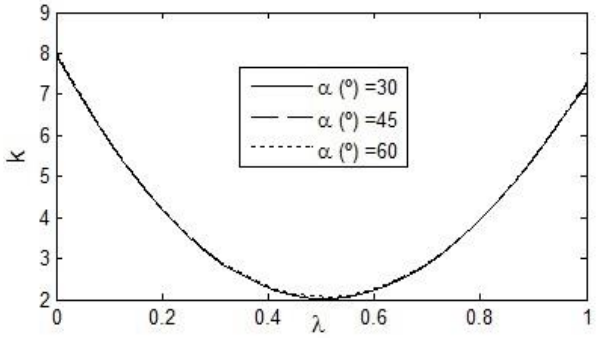

***Figure 8**: Influence of geometric parameters λ and α on the normalized rotational stiffness of bearing loaded with pure bending moment*

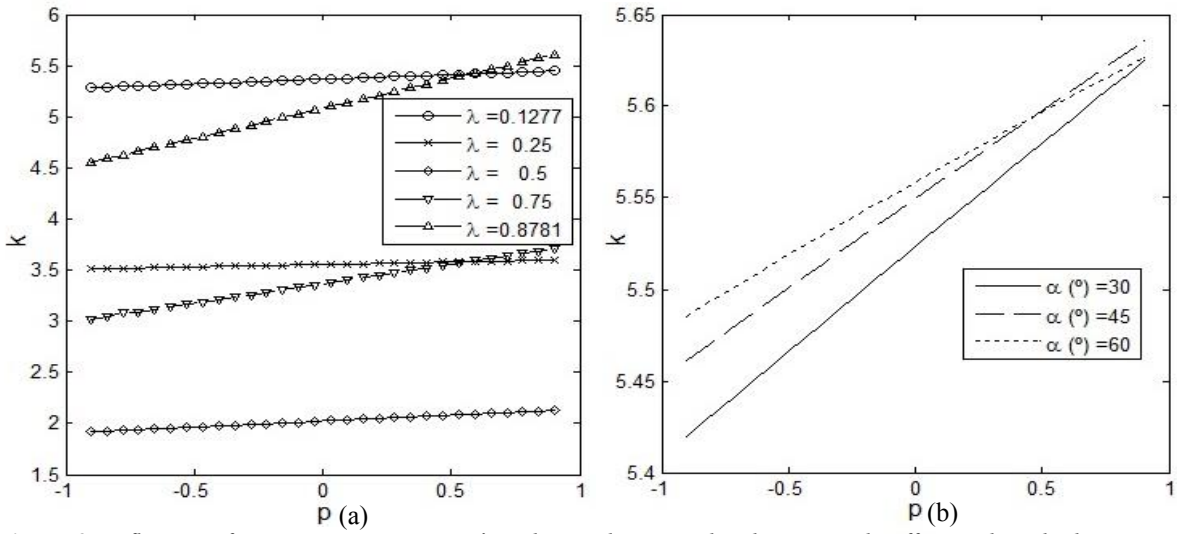

***Figure 9**: Influence of geometric parameters λ and α on the normalized rotational stiffness when the bearing is submitted to action of the vertical load p - (a) k against p for λ=0.1277, 0.25, 0.5, 0.75 and 0.8781 and α=45°, (b) k against p for α=30°,45ª and 60° and λ=0.1174*

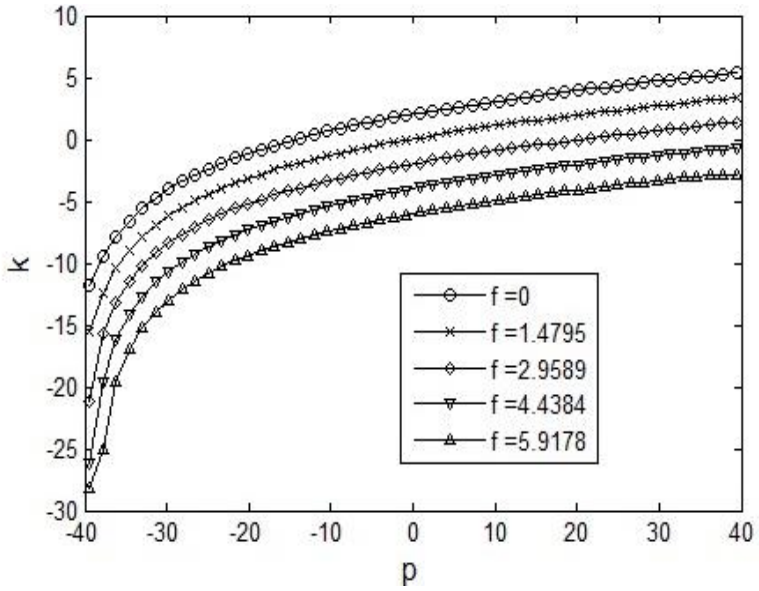

***Figure 10**: Influence of the normalized horizontal load on the normalized rotational stiffness*

3.4 Stress analyzes

The bearing motion capability is determined by stress developed on its leaves. Due to the bearing nonlinear behavior, it is a complex task to obtain a direct correlation between stress and rotational angles [5]. Thus, to determine whether the bearing support a specific rotational angle the most critical stress point on the leaves should be compared to the allowable stress (ratio between the yield strength stress of the material and safety factor).

Once the leaves of cross-spring bearings are slender it is possible to assume a plane strain state acting on them. Then, stress distribution along the leaves may be written superposing the axial stress and the bending stress. In this case, the shear stress can be neglected since the length of each leaf is far greater than its thickness.

Axial stress is constant along the leaf and can be expressed as:

$$\sigma_{ia} = \frac{Ep_i}{s}, \; i = 1,2 \tag{25}$$

On the other hand, the bending stress along the length of the leaf is given by:

$$\sigma_{if}(x_i, y_s) = \frac{-\sqrt{3}Em_i(x_i)y_s}{\sqrt{s}},\ i = 1,2 \tag{26}$$

Eq. 26 shows that the bending stress is function of the internal bending moment, which can be written as:

$$m_i(x_i) = -p_i\left[\delta y_i - y_i\left(x_i\right)\right] + f_i\left(1 - x_i\right) + m_i,\ i = 1,2 \tag{27}$$

Then, superposing the effects, the resulting stress along the length of the leaf is expressed by:

$$\sigma_i(x_i, y_s) = -\frac{-\sqrt{3}Em_i(x_i)y_s,}{\sqrt{s}} + \frac{Ep_i}{s},\ i = 1,2 \tag{28}$$

When p_i is positive the neutral axis of the leaf displaces downward so that the maximum stress on each section is a tensile stress. On the other hand, if p_i is negative, the maximum stress is of compression.

For the sake of giving a better insight in the comparison between the critical stress developed on the leaves and the allowable stress, unlike the previous analyzes, this parameter is expressed in the dimensional form herein. Then, shape parameters of the leaves and material property should be given to perform analyzes.

Nevertheless, in order to compare the results obtained by the proposed model with those provided by the literature [5], shape parameters and material property were conveniently chosen as showed by tables 1 and 2.

***Table 1**: Shape parameters of the leaves and Young's modulus provided by* [5]

L (mm)	***b (mm)***	***t (mm)***	***E (Pa)***
60	6	0.5	$73x10^{11}$

***Table 2**: Geometric parameters of 3 cross-spring bearings provided by* [5]

Bearing Nr.	***λ***	***α(º)***
1	0.1277	30
2	1/3	45
3	0.5	45

Figures 11 and 12 show that although the stress along the leaves be influenced by the bearing geometry (see also Figures 13 and 14) the critical stress always occurs on one end of the leaves, when the bearing is loaded by pure moment [5]. It is also possible to note that the effect of the axial stress is far less than the bending stress, once the neutral axis deviation is negligible so that the compressive and tensile stress distribution are practically symmetric.

Furthermore, Figure 12 shows that the symmetric bearing produces the smallest critical stress since the stress distributions along the leaves in this case are nearly constant. The same conclusion can be obtained from Figure 13 which shows that when λ is 0.5 the critical stresses developed on each end of the leaves are almost the same. Curves from Figure 13 also show that for symmetric correspondent bearings (e.g. λ=0.1277 and 0.8781) loaded by pure moment the critical stress occurs at opposite ends of the leaves. Finally the comparison between the

results provided by [5] and those achieved by the proposed model showed to be in excellent agreement when λ influence is evaluated. In case, it was assumed α=45º.

Regarding the evaluation of the α parameter it is possible to note that this parameter has almost no influence on the stress distribution on the end of the leaves when the bearing is symmetric and poorly influence when λ is 1/3, in case of pure bending moment, see Figure 14 (a) and (b) respectively. In addition, analyze from curves of Figures 13 and 14 show, as expected, that the influence of the geometric parameter λ in the stress on end of the leaves is far greater than the influence of α. When the results presented by [5] and those obtained by the prosed model are compared it is possible to note a good agreement when λ is 1/3 and only a reasonable concordance when λ is 0.5, see Figures 14 (a) and (b), respectively. In all of these cases a rotational angle of 15º was applied to the moving member of the bearing.

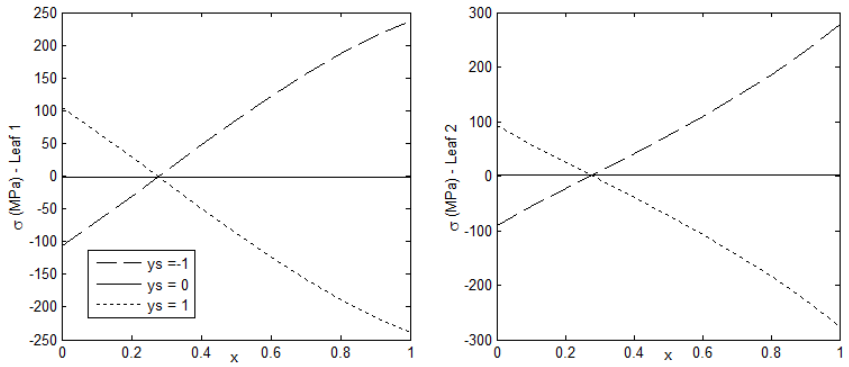

***Figure 11**: Stress distribution along the normalized length of leaves 1 and 2 of the bearing 1*

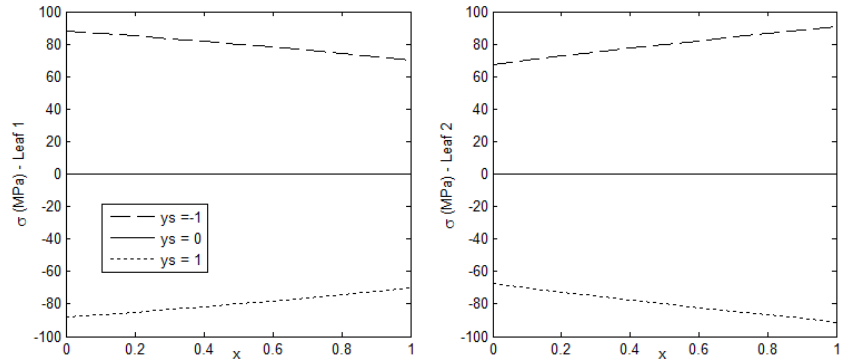

***Figure 12**: Stress distribution along the normalized length of leaves 1 and 2 of the bearing 3*

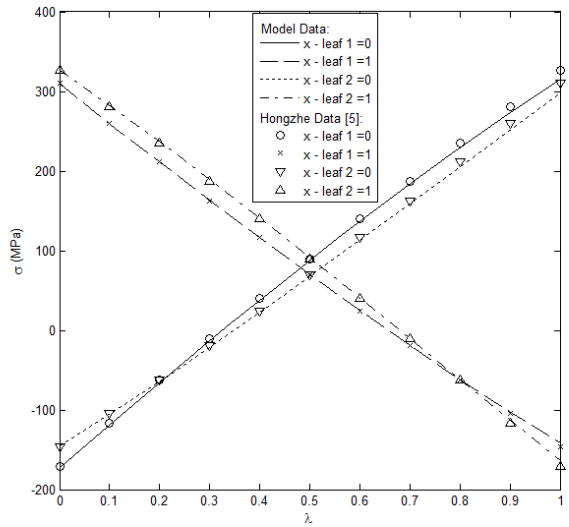

***Figure 13**: Influence of geometric parameter λ on the stress at two ends of the leaves when the bearing (α=45ª) is loaded by pure bending moment*

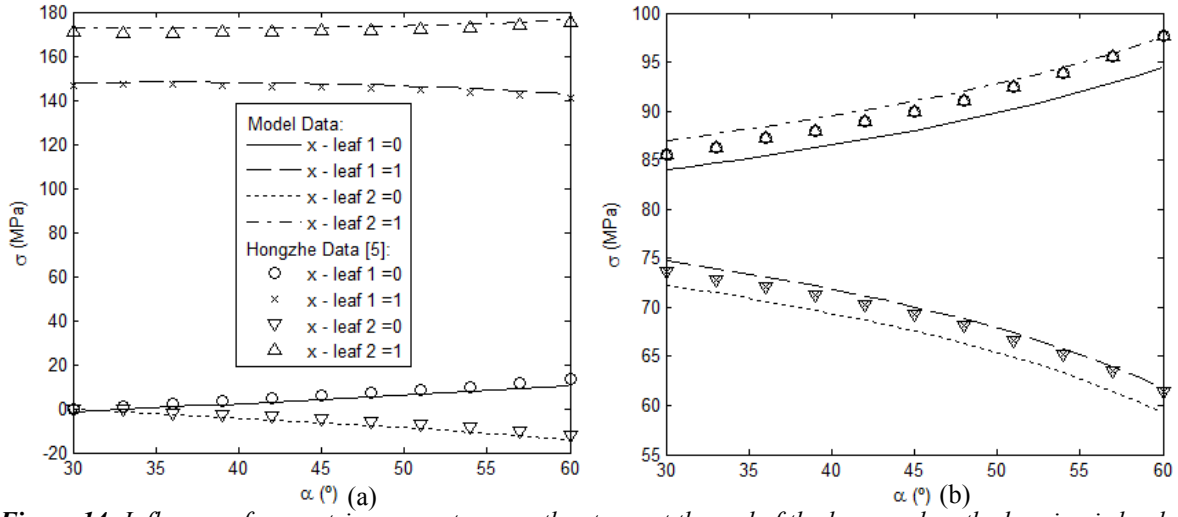

***Figure 14**: Influence of geometric parameter α on the stress at the end of the leaves when the bearing is loaded by pure bending moment – (a) bearing with λ=1/3, (b) bearing with λ=0.5*

Analyzes taking into account the influence of the vertical load on the stress distribution along the length of the leaves are presented in the next section.

4. FEA VERIFATION

With the aim of checking the consistency of the results presented by the model proposed in the section 2 it was performed FEA using the well-known Finite Element software ANSYS 14.0. Analyzes were carried out using the element, based on Timoshenko Beam Theory, BEAM188 which has six degree of freedom on each node. Besides that, this element is able to capture the complex bearing behavior properly because it includes geometric nonlinearity (large-rotation and displacement capability) on its formulation.

In order to establish the comparison, not only between the FEA and the results provided by the proposed model for each bearing, but also among the several bearing geometric configurations it was adopted for all analyzes an angle θ of the moving varying from 0º up to 15º and the vertical load P assuming three distinct values: -4N, 0 and 4N. Furthermore horizontal loads were not used because, as described in the previous section, they have less importance on most practical applications.

Tables 3 shows the bearing shape parameters and material property while in table 4 are listed the bearings that were used in the FEA verification.

***Table 3**: Shape parameters of the leaves and Young's modulus*

L (mm)	*b (mm)*	*t (mm)*	*E (Pa)*
40	6	0.5	$73x10^{11}$

***Table 4**: Geometric parameters of 8 cross-spring bearings provided*

Bearing Nr.	*λ*	*α (º)*
1	0.1277	45
2	0.1277	60
3	1/3	45
4	1/3	50.77
5	0.43	60
6	0.5	45
7	0.82	45
8	0.8781	30

4.1 Rotary axis deviation

Figures 15 and 16 show the rotary axis deviation and their components for the bearings 1 and 2 respectively. First of all, it is worth to note that Y component of the axis deviation in these two geometric configurations are greatly influenced by the presence of the vertical load P. It occurs because this component is dominated by a high order term (θ^4 order), namely it is nearly to zero when the bearings with $\lambda = 0.1277$ undergo a pure moment condition of load [3]. It also obvious to see that a positive value of P displaces the Y component downward, it means, in the positive direction whereas negative P displaces this component upward. Thus, the effect of the Y displacement component, due to the presence of the vertical load, is consequently transmitted to the resultant deviation D.

On the other hand, Hongzhe and Shusheng [3] show that X component of the axis deviation of cross spring bearings is of θ^3 order so that it domains the resultant deviation D, on configurations of Figures 15 and 16 when the bearing is loaded with pure bending moment. Furthermore, as intuitively expected, the vertical load P has small influence over this component.

When λ is 0.5 (bearing 6) the vertical load P has small influence on the components X and Y of the rotary axis deviation, see Figure 17. It may be a useful characteristic for application in which strong variations of the axis deviation behavior due to the presence of this load is undesirable.

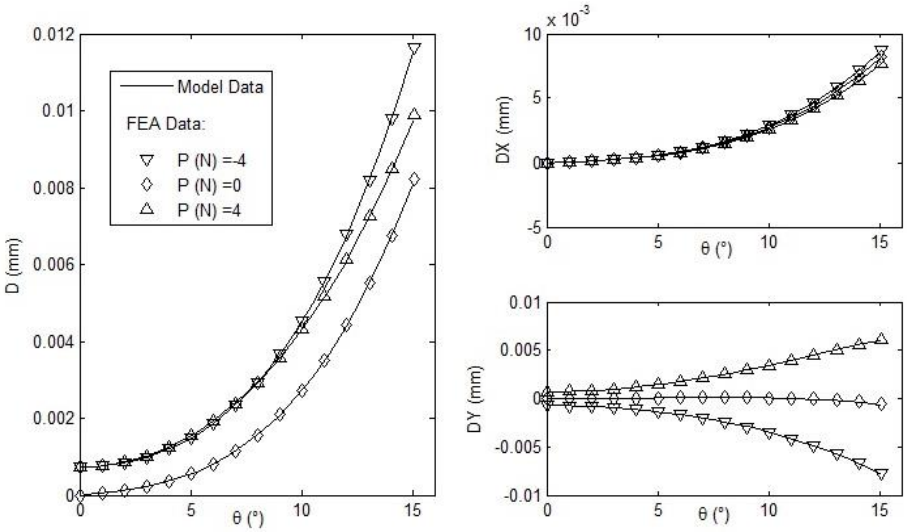

***Figure 15**: Rotary axis deviation and its components of the bearing 1*

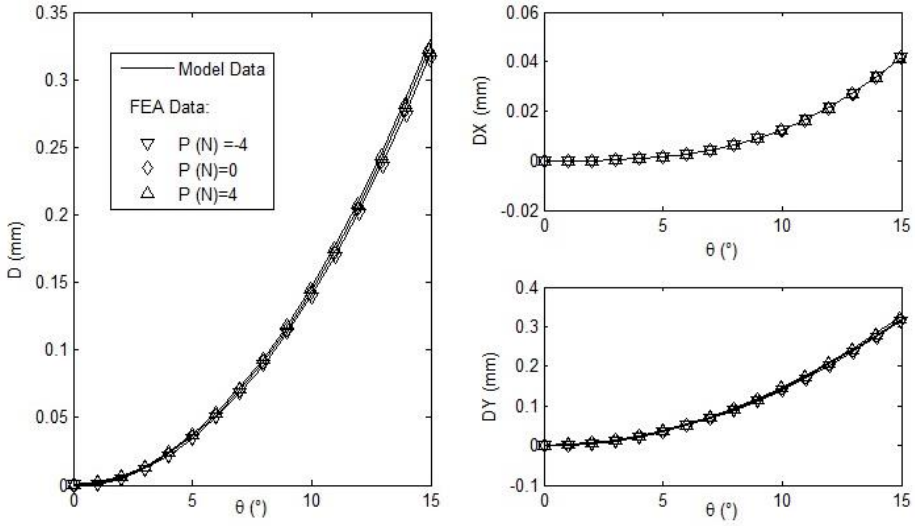

***Figure 16**: Rotary axis deviation and its components of the bearing 2*

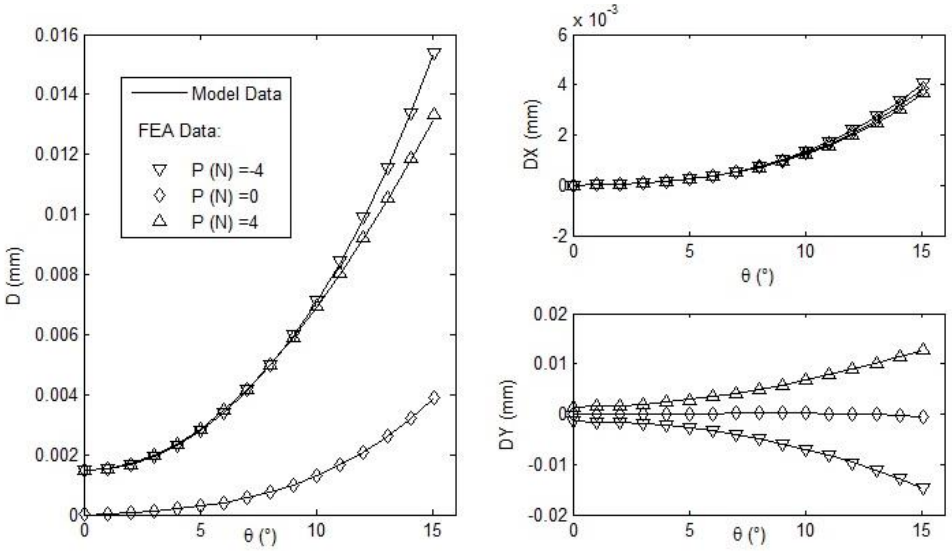

***Figure 17**: Rotary axis deviation and its components of the bearing 6*

The evaluation of Figures 15, 16 and 17 confirm that the geometric parameter λ has a far greater influence on the axis deviation than the parameter α, regardless the condition of load acting on the bearing.

In addition, it is possible to see for these configurations a very good agreement between the results provided by the FEA and those obtained by the proposed model even when the axis deviation is dominated by the terms of high order and large angles of rotation (up to 15º) are used. It was reached on these cases a maximum relative deviation of 4.5% between the results reaming in most cases less than 2%.

Unlike aforementioned analyzes, the comparison between the FEA and the results obtained for the bearing 8 shows only a reasonable agreement, in small angles of rotation, see Figure 18. It occurs because the rotary axis deviation in this case, as when λ is 0.1277, is greatly diminished so that the mathematic model was not accurate enough to capture its effect properly for large rotational angles.

Hongzhe and Shusheng [3] extend this conclusion saying that the model proposed by them is not able to capture high order terms (θ^3 and θ^4 orders for X and Y components respectively) when λ is greater than 0.5. To overcome this limitation they propose, taking into account symmetry considerations, a transformed bearing which must satisfy new boundary and initial conditions.

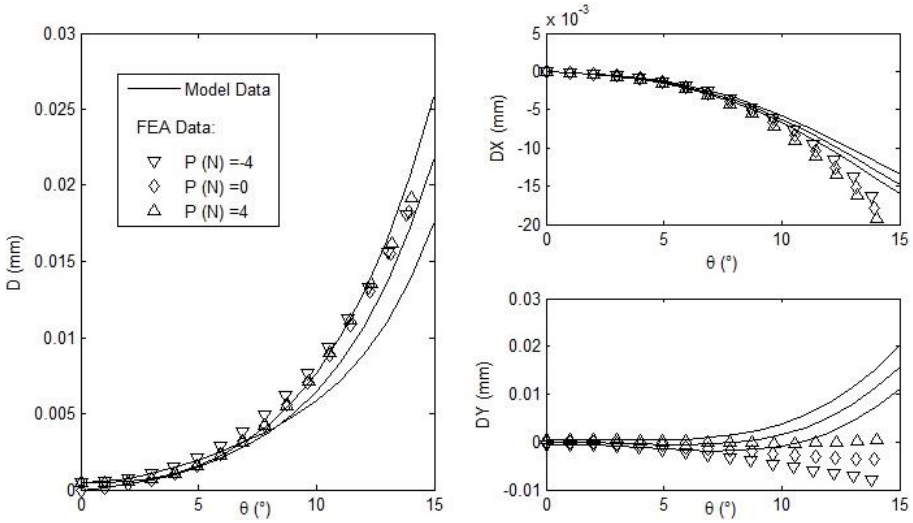

***Figure 18**: Rotary axis deviation and its components of the bearing 8*

However for rotational angles up to 5º a reasonable accuracy was reached; in case a maximum relative deviation between the results of less than 8.5%. Despite being small this range for the rotational angle fulfill most of the practical applications, so that the applicability of the proposed mathematic model is not invalidated even when λ is 0.8781 or values in its vicinity are adopted.

Finally, comparison among the bearings from Figures 15, 16, 17 and 18 confirm that λ=0.5 produces the greatest axis deviation, which can be, for rotational angles up to 15º and the P load varying between -4 and 4N, until 100 times greater than those deviations produced by the geometric configurations of λ=0.1277 and 0.8781.

4.2 Stiffness Characteristics

The stiffness of cross-spring bearings, as defined in the previous section, is an important parameter for evaluation of the load-rotation relationship of such device. Unlike the already performed analyzes, curves in this section are given by the external moment applied to the bearing moving member as function of its rotational angle. Figures 20 and 21 show that curves present a nearly linear behavior so that the stiffness can be understand as the angular coefficient of these straight lines.

First of all, the analysis from curve illustrated in Figure 19 (b) show that bearing 4 presents a constant rotational stiffness regardless the magnitude of the vertical load applied. On the other hand, bearing 3 with a semi-angle between the leaves just 5.77º smaller than that of the bearing 4, displays a stiffness that varies as function of the vertical load magnitude, see Figure 20 (a).

According to Hongzhe and Shusheng [5] the stiffness of cross spring bearings with geometric configuration that satisfies Eq. 29 are not influenced by external vertical load P.

$$\cos^2 \alpha = \frac{-2(9\lambda^2 - 9\lambda + 1)}{15\lambda} \tag{29}$$

Where:

$$\lambda \in \left(\frac{1}{2} - \frac{\sqrt{5}}{6}, \frac{1}{2} + \frac{\sqrt{5}}{6} \right) \text{ and } \alpha \in \left(\arccos\sqrt{\frac{2}{5}}, \frac{\pi}{2} \right)$$

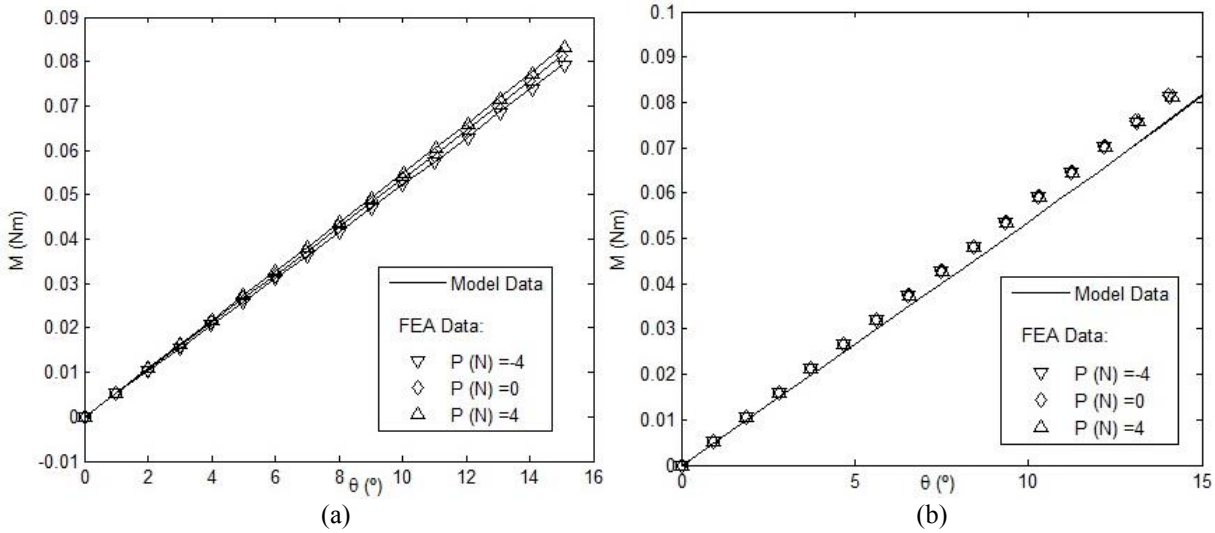

***Figure 19**: Rotational stiffness characteristics - (a) bearing 3, (b) bearing 4*

These particular geometries may be very useful in practical applications, in which a large range of variation of the P load is required.

In addition, curves from Figures 20 (a) and (b) show that depending on the bearing geometric configuration the stiffness can be reduced by effect of a compressive vertical load (bearing 7) or increased (bearing 5). Reciprocally, when a tensile vertical load is applied the inverse behavior occurs.

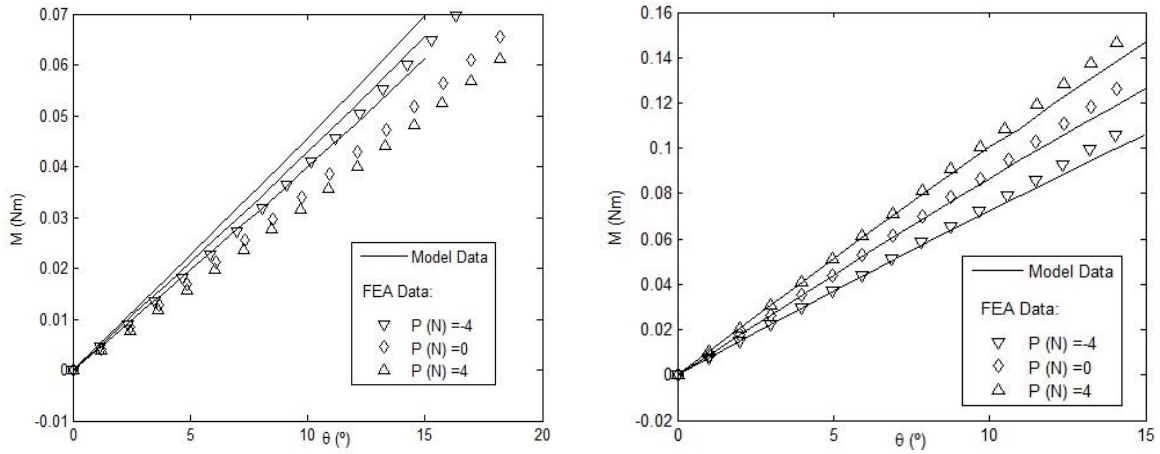

***Figure 20**: Rotational stiffness characteristics - (a) bearing 5, (b) bearing 7*

Finally, the comparison between the FEA and the results achieved by the model for the bearings 3, 4 and 7 are in good agreement, with a maximum relative deviation less than 7.2% for rotational angles up to 15º, whereas those obtained for the bearing 5 are less accurate.

4.3 Stress Analyzes

The analyzes presented in this section intent the comparison of the results provided by the FEA and those obtained by the proposed model for the stress distribution along the leaves when the vertical load P is applied to the bearing.

Figure 21 show that the presence of the vertical load may influence strongly the stress distribution along the leaves. In fact, when the vertical load is compressive and large enough it displaces the critical point from the end of the leaf to an intermediary point on it [5], as occurred when a vertical load of -4N was applied to the bearing 6. On the other hand, when the vertical load is a tensile load the critical stress always occurs on the end of the leaves, regardless of its magnitude.

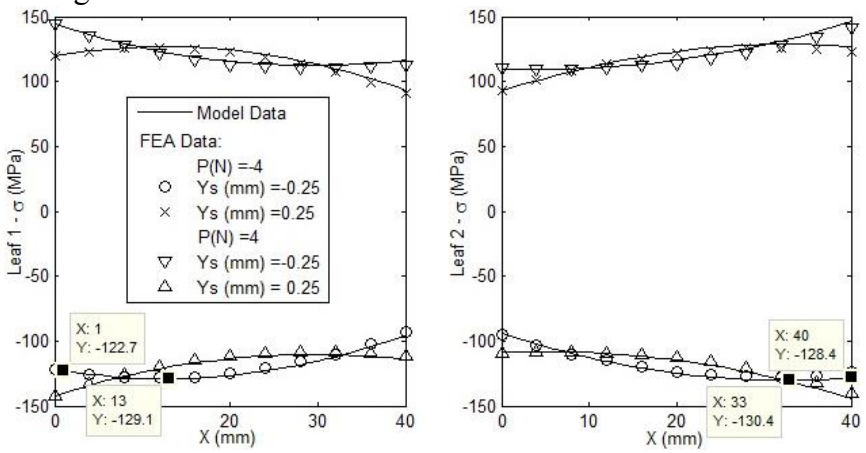

***Figure 21**: Stress distribution along the length of leaves 1 and 2 of the bearing 6 when it is submitted to external vertical loads P of 4N and 4N*

Finally comparison between FEA and the results provided by the proposed model shows an excellent agreement with a maximum relative deviation less than 0.5%.

5. CONCLUSION

In this work was presented an alternative approach to model the elasto-kinematic characteristics of generalized cross-spring bearings. An analytical formulation was performed and a numeric-iterative technique was used to solve the resulting nonlinear system.

It was shown that the rotary axis deviation of cross-spring bearings is substantially diminished when λ is 0.1277 or 0.8781, for the case in which the bearing is loaded with pure moment. However, the Y component and also the rotary axis deviation are strongly affected by the presence of a vertical load, especially when λ is 0.1277 or 0.8781, because, for a pure moment condition of load, this component is nearly to zero on these points (high order term domination). Thus, the minimum rotary axis deviation displaces so that an optimized geometric configuration is not possible to be established when variations of the vertical load occur. In these cases, a reasonable geometric configuration was proposed by tanking the average of the optimal λ values produced by the maximum and minimum magnitude of p. This approach should be carefully evaluated and applied just for the cases in which the discrepancy between the optimal λ values is small.

Regarding the rotational stiffness of cross spring bearings it was shown that the stability of such bearings can be predicted by the evaluation of this parameter, so that when the bearing assume a negative stiffness it becomes geometrically unstable.

Results provided by the model also reveal that for symmetric bearing configuration (λ=0.5) the compliance is a maximum (smallest rotational stiffness).

In addition, it is noteworthy that stiffness is substantially decreased when the bearing is loaded by horizontal load, regardless the bearings geometric configuration. Depending on the magnitude of this load the stiffness can become negative, so, for most practical applications its use should be avoided.

On the other hand, the influence of the vertical load on the rotational stiffness is dependent on the bearing geometric configuration. Thus, a positive vertical load can decrease, increase or not alter the stiffness. A similar behavior is verified to the negative vertical load.

The stress developed on the leaves determines the motion capability of cross spring bearings. Thus, the stress distribution along the leaves was also evaluated. It was shown that when the bearing is loaded by pure moment the critical stress occurs on one end of the leaves. However, when a compressive load is present the critical stress may be displaced to an intermediary point of the leaves.

The stress analyzes also showed that the symmetric configuration of the bearing (λ=0.5) produces a nearly constant stress distribution and the smallest critical stress magnitude.

Furthermore, analyzes of the influence of the geometric parameters showed that λ affects more the rotary axis deviation, rotation stiffness and the stress distribution along the leaves than α.

Finally results verified by FEA showed to be in good agreement even for large angles of rotation (up 15º). An exception occurred for the rotary axis deviation of the bearing with λ=0.8781, in which the results fit well only for rotational angles up to 5º.

6. ACKNOWLEDGMENTS

These results were achieved in the research project DINTOR, a sub-project of the German-Brazilian BRAGECRIM Research Initiative, funded by DFG (German Research Foundation) and CAPES (Brazilian Research Foundation)

7. REFERENCES

[1] A. C. P. Bitencourt, R. Theska, A. Wagner, H. A. Lepikson, and L. A. Gonçalves Junior, "A novel approach in the application of flexure bearings in primary torque standard machines," in *Proceedings of 11th euspen International Conference*, 2011.

[2] A. C. P. Bitencourt, L. A. Gonçalves Junior, and R. Theska, "A novel mathematical model for flexure bearings applied in primary torque standard machines," in *Proceedings of 21st International Congress of Mechanical Engineering*, 2011.

[3] Z. Hongzhe and B. Shusheng, "Accuracy characteristics of the generalized cross-spring pivot," *Mechanism and Machine Theory*, vol. 45, no. 10, pp. 1434–1448, 2010.

[4] X. Pei, J. Yu, G. Zong, and S. Bi, "An effective pseudo-rigid-body method for beam-based compliant mechanisms," *Precis. Eng.*, vol. 34, no. 3, pp. 634–639, 2010.

[5] Z. Hongzhe and B. Shusheng, "Stiffness and stress characteristics of the generalized cross-spring pivot," *Mechanism and Machine Theory*, vol. 45, no. 3, pp. 378–391, 2009.

[6] B. D. Jensen and L. L. Howell, "The modeling of cross-axis flexural pivots," *Mechanism and Machine Theory*, vol. 37, no. 5, pp. 461–476, 2002.

[7] W. Wittrick, "The theory of symmetrical crossed flexure pivots," *Australian Journal of Scientific Research*, vol. A1, no. 2, pp. 121–34, 1948.

[8] S. Zelenika and F. De Bona, "Analytical and experimental characterisation of high-precision flexural pivots subjected to lateral loads," *Precision Engineering*, vol. 26, no. 4, pp. 381–388, 2002.

[9] L. A. Gonçalves Junior, "Caracterização do comportamento elastocinemático de mancais flexíveis de lâminas cruzadas" *Bachelor Thesis*, *Universidade Federal da Bahia, Brazil*, 2013.

[10] W. Wuest, "Blattfedergelenke für Meßgeräte," *Feinwerktechnik*, vol. 54, no. 7, pp. 167–70, 1950.

[11] J. a. Haringx, "The cross-spring pivot as a constructional element," *Applied Science Research*, vol. A1, no. 1, pp. 313–332, 1949.

[12] S. Awtar, A. H. Slocum, and E. Sevincer, "Characteristics of Beam-Based Flexure Modules," *ASME Journal of Mechanical Design*, vol. 129, no. 6, p. 625-639, 2007.

[13] S. Roweis, "Levenberg-marquardt optimization," *University of Toronto*, 1996.

8. RESPONSIBILITY NOTICE

The authors are only responsible for the printed material included in this paper.

